International Journal of Nanomedicine

Dovepress

open access to scientific and medical research

Open Access Full Text Article

ORIGINAL RESEARCH

Size-Optimized Layered Double Hydroxide Nanoparticles Promote Neural Progenitor Cells Differentiation of Embryonic Stem Cells Through the Regulation of M^{6}A Methylation

Yuxin Bai[1,2], Yanjing Zhu[1], Xiaolie He[1], Ruiqi Huang[1,2], Xu Xu[1], Li Yang[1], Zhaojie Wang[1,2], Rongrong Zhu[1,2]

[1]Key Laboratory of Spine and Spinal Cord Injury Repair and Regeneration of Ministry of Education, Department of Orthopedics, Tongji Hospital Affiliated to Tongji University, School of Life Science and Technology, Tongji University, Shanghai, 200065, People's Republic of China; [2]Frontier Science Center for Stem Cell Research, Tongji University, Shanghai, 200065, People's Republic of China

Correspondence: Zhaojie Wang; Rongrong Zhu, Email 2013wangzhaojie@tongji.edu.cn; rrzhu@tongji.edu.cn

Purpose: The committed differentiation fate regulation has been a difficult problem in the fields of stem cell research, evidence showed that nanomaterials could promote the differentiation of stem cells into specific cell types. Layered double hydroxide (LDH) nanoparticles possess the regulation function of stem cell fate, while the underlying mechanism needs to be investigated. In this study, the process of embryonic stem cells (ESCs) differentiate to neural progenitor cells (NPCs) by magnesium aluminum LDH (MgAl-LDH) was investigated.

Methods: MgAl-LDH with diameters of 30, 50, and 100 nm were synthesized and characterized, and their effects on the cytotoxicity and differentiation of NPCs were detected in vitro. Dot blot and MeRIP-qPCR were performed to detect the level of m^{6}A RNA methylation in nanoparticles-treated cells.

Results: Our work displayed that LDH nanoparticles of three different sizes were biocompatible with NPCs, and the addition of MgAl-LDH could significantly promote the process of ESCs differentiate to NPCs. 100 nm LDH has a stronger effect on promoting NPCs differentiation compared to 30 nm and 50 nm LDH. In addition, dot blot results indicated that the enhanced NPCs differentiation by MgAl-LDH was closely related to m^{6}A RNA methylation process, and the major modification enzyme in LDH controlled NPCs differentiation may be the m^{6}A RNA methyltransferase METTL3. The upregulated METTL3 by LDH increased the m^{6}A level of *Sox1* mRNA, enhancing its stability.

Conclusion: This work reveals that MgAl-LDH nanoparticles can regulate the differentiation of ESCs into NPCs by increasing m^{6}A RNA methylation modification of *Sox1*.

Keywords: mouse embryonic stem cell, neural progenitor cells, layered double hydroxide nanoparticles, size-dependent, differentiation, m^{6}A RNA methylation

Introduction

Embryonic stem cells (ESCs) characterized by self-renewal and pluripotency are derived from the inner cell mass (ICM) of the blastocyst and capable of differentiating into several neural cells with appropriate external induction.[1] ESC-derived neural precursor cells (NPCs) with self-renewal and the capacity of differentiating into various neural cells have been successfully transplanted into the injured region of the central nervous system (CNS) so as to be applied in the therapy of neurodegenerative diseases and nerve damage.[2] NPCs derived from ESCs were transplanted into injured spinal cord of rats or nonhuman primate, and these transplanted neurospheres contributed to the functional recovery of spinal cord injury.[3,4] The transplantation of ESC-derived NPCs could efficiently reconstruct the injured neural tissues and improve

Received: 6 February 2024
Accepted: 2 May 2024
Published: 13 May 2024

brain functions of stroke-damaged rats.[5] Hence, it holded immense significance to explore innovative strategies and relevant mechanisms regulating the differentiation of ESCs into NPCs.

Several protocols inducing differentiation of ESCs into NPCs in vitro had been optimized for years, which played a nonnegligible role in the regulation of stem cell fate. ESCs spontaneously formed specific embryoid bodies (EBs) containing cells of the three germ layers after removal of factors that sustained pluripotency, and nerve cells were then proliferated in a specific selective medium.[6] This method was based on the spontaneous differentiation of cells with a large number of indefiniteness. Moreover, EBs contained cell types of three germ layers and the maturity of neural cells was inconsistent, which was not conducive to the transplantation and repair of neural damage.[7] Co-culturing mESCs with stromal cells, such as PA6 and MS5, significantly enhanced neural differentiation of mESCs, but the differentiated products could be contaminated by unknown components of feeder cells, which was unfavorable for further research on signaling pathways during differentiation.[8] Committed differentiation of ESCs by supplementing specific inducing factors without serum and conditioned medium was not be interfered by exogenous cells, and a high proportion of NPCs could be obtained.[9] The neural differentiation of ESCs regulated by supplementing the medium with specific exogenous factors such as nanomaterials, growth factors, and retinoic acid (RA) had been widely investigated.[10,11] Nanomaterials with stable physicochemical properties were easily synthesized and modified, promising for regulating neural differentiation of stem cells.[12–15] Taken together, investigation of nanomaterials regulating the differentiation of ESCs into NPCs could offer theoretical basis for cell fate regulation of biomaterials in ESCs.

The size of nanomaterials similar to that of biomolecules facilitated their penetration of various biomembrane and interactions with DNA or proteins in organs, tissues, or cells, thereby affecting physiological processes in vivo.[16] Increasing evidences indicated that the neural differentiation of ESCs could be promoted by nanomaterials with stable physicochemical properties in recent years.[12,17,18] mESCs could be effectively differentiated into neural precursors, neurons, astrocytes, and oligodendrocytes supported by nanofibrous poly(lactic-co-glycolic acid) (PLGA) 3D scaffolds, and the fraction of NPCs on PLGA aligned nanofibers was significantly higher than that of PLGA random nanofibers.[19] Encapsulating the neural differentiation factor RA in a mesoporous silica nanoparticle (MSN) significantly facilitated the neural differentiation of mESCs.[20] Neural differentiation-related functional units (glyco and sulfonate units) anchored on the gold nanoparticles (GNP) surface were transferred to the surface of cell membrane via GNP-membrane interactions, thereby promoting differentiation of ESCs into neuronal lineages more effectively.[21] Nervous system treatment can benefit from the use of nanocomposites due to their low toxicity in central nervous system and their ability to produce profound recovery effects. However, the majority of these effects are derived from loaded factors, and few of these nanomaterials possess immunoinhibitory properties. Furthermore, the underlying mechanisms by which these biomaterials regulate the fate of stem cells remain elusive.

Layered double hydroxide (LDH) nanoparticles, a sort of anionic hydrotalcite-like clays, possess a range of exceptional biological characteristics, such as favorable biocompatibility, pH sensitivity, secure biodegradation, and anti-inflammatory properties, contributing to their extensive investigation in the field of immune response regulation and stem cell fate regulation.[22] Previous research discovered that they play a key role in sustaining the stemness of mESCs, neural regeneration and suppressing the expression of inflammatory factors.[23–25] However, there are few reports on the regulation of neural precursor differentiation of embryonic stem cells by LDH. This work initially investigated the effects of LDH on the fate of NPCs and revealed that 100 nm LDH could significantly accelerate the process of NPCs differentiation. The specific molecular mechanism of LDH promoting NPCs differentiation needed to be further studied.

N^6-methyladenosine (m^6A) is a common modification type on eukaryotic mRNA, regulated by "writing" proteins (METTL3, METTL14, and WTAP), "erasing" proteins (FTO and ALKBH5), and "reading" proteins (YTH family proteins and IGF2BP family members).[26–28] Researches have shown that m^6A methylation modification can affect RNA function by regulating RNA stability, recognizability, and translation efficiency.[29] During the differentiation process of stem cells, m^6A methylation modification can regulate gene expression, thereby affecting the differentiation fate of cells.[30] It had been found that m^6A RNA modification that could affect the fate of mESCs was enriched in numerous core regulators that maintained pluripotency of mESCs, and the absence of RNA methylation affected the chromatin stability of ESCs and prevented them from naïve to primed state, thereby inhibiting differentiation of cells.[31–33] In this work, whether LDH promotes NPC differentiation through m^6A modification was explored. Interestingly, our results

demonstrated that LDH nanoparticles could significantly facilitated NPCs differentiation of mESCs by upregulating the expression level of m^6A RNA methyltransferase METTL3, a component of m^6A methylase complex.

Based on the regulatory role of m^6A methylation modification on the fate of mESCs and the preliminary results showing that m^6A level gradually increased during NPCs differentiation and LDH up-regulated the expression of METTL3, we proposed a hypothesis that LDH affected the differentiation process of NPCs by regulating the level of m^6A in specific genes.

Materials and Methods

Synthesization and Characterization of Nanoparticles

The 100 nm MgAl-LDH was synthesized by a coprecipitation and subsequent hydrothermal method. $Al(NO_3)_3{\cdot}9H_2O$, $Mg(NO_3)_2{\cdot}6H_2O$, and NaOH were supplied by Sinopharm Group Co. Ltd. Typically, 0.544 g NaOH was dissolved into 60 mL deionized water (ddH_2O) under N_2 atmosphere, vigorously stirred at 1000 rpm, and then 1.538 g $Mg(NO_3)_2{\cdot}6H_2O$ and 0.75 g $Al(NO_3)_3{\cdot}9H_2O$ dissolved into 40 mL ddH_2O were added in the stirring NaOH solution at room temperature for 20 min. The product was washed three times by ddH_2O, dispersed into 70 mL ddH_2O and hydrothermally placed in a 100°C autoclave for 16 h. The obtained sediment was then washed thrice by ddH_2O, and finally MgAl-LDH was obtained. 30 nm MgAl-LDH nanoparticles were obtained by replacing the solvent of $Al(NO_3)_3{\cdot}9H_2O$, $Mg(NO_3)_2{\cdot}6H_2O$, and NaOH with methanol, and the subsequent material synthesis procedure was the same as 100 nm LDH.

To synthesize 50 nm MgAl-LDH, a 20 mL mixed aqueous solution of 1.538 g $Mg(NO_3)_2{\cdot}6H_2O$ and 0.75 g $Al(NO_3)_3{\cdot}9H_2O$ was prepared. The pH of the mixture was adjusted to 10.0 by NaOH aqueous solution, followed by vigorously stirring for 5 h at 80°C. The 50 nm MgAl-LDH was obtained by centrifugation, washed, and resuspended in ddH_2O.

The morphology of MgAl-LDH was obtained using transmission electron microscope (TEM). The Malvern Nano Zetasizer series was applied to determine Zeta potential of MgAl-LDH. X-ray photoelectron spectroscopy (XPS) was applied to detect the elemental content of MgAl-LDH. X-ray diffraction (XRD) was applied to detect the crystal structure of MgAl-LDH.

Cell Culture

The mESC line 46C was purchased from National Collection of Authenticated Cell Cultures. High-glucose DMEM medium (Gibco) added with 1000 U mL^{-1} LIF (1000 U mL-1), 1% penicillin and streptomycin (Gibco), 1% NEAA (Gibco), 1% glutamax (Gibco), 1% sodium pyruvate (Gibco), 0.1 mM β-mercaptoethanol (Gibco), and 15% FBS (Gibco) was applied to culture mESCs on feeders spreaded over gelatin. The medium was changed daily, and mESCs were passaged approximately every 2~3 days. For the differentiation of mESCs into NPCs, a density of 5×10^4 cells mL^{-1} cultured with NPCs medium (G-MEM (Gibco) supplemented with 1% penicillin and streptomycin, 1% NEAA, 1% glutamax, 1% sodium pyruvate, 0.1 mM β-mercaptoethanol, and 8% Knockout serum replacement) were suspended in ultra low attachment plates. The MgAl-LDH was supplemented on the third day of differentiation. NPCs were passaged every 3 days, and the medium was changed every other day.

CCK-8 Test

Cell counting kit-8 (CCK-8) (APExBIO, Houston, USA) was applied to assess the viability of cells treated with 10~40 μg mL^{-1} MgAl-LDH of different sizes according to the instruction of test kits. Cells treated with MgAl-LDH of different sizes were grown in the incubator for 72 h. Cells were transferred to a 96-well plate at a density of 1×10^4 cells $well^{-1}$ and incubated with CCK-8 solution in the incubator for an additional 2 h. A microplate reader at 450 nm was used to detect the absorbance. The cell survival rate was calculated as OD (experimental group)/OD (blank control group) × 100%.

Cell Apoptosis Analysis

The Annexin V-APC/7-AAD apoptosis detection kit (KeyGEN BioTECH, Nanjing) was selected to analyze cell apoptosis. Cells were treated with 40 μg mL^{-1} MgAl-LDH nanoparticles of different sizes for 72 h. Cells trypsinized

were washed with PBS and incubated with a prepared mixture including 5 μL Annexin V-APC, 5 μL 7-AAD, and 500 μL binding buffer for 15 min without light. Flow cytometer was applied to detect cell apoptosis. The results were analyzed by Flowjo software.

Cell Cycle Analysis

Cells were treated with 40 μg mL^{-1} MgAl-LDH of different sizes for 72 h. After trypsinization, single cells were fixed with 500 μL cold 70% ethanol at 4°C for 4 h, centrifuged to discard 70% ethanol, resuspended with prepared 500 μL PI/RNase A (KeyGEN BioTECH, Nanjing) for 30 min without light, and analyzed by flow cytometry.

EdU Detection

Cells proliferation was analysed by EdU detection kit (APExBIO, Houston, USA). Spheres treated with 40 μg mL^{-1} MgAl-LDH of different sizes for 72 h were incubated with 10×10^{-6} M EdU solution for 3 h, fixed in 4% PFA for 30 min, permeabilized in 0.5% Triton X-100 for 20 min, incubated with prepared Click-iT working buffer for 30 min without light, stained by DAPI in dark for 10 min, and finally the fluorescence intensities of EdU was photographed by confocal laser scanning microscope. Spheres incubated with 10×10^{-6} M EdU solution for 3 h were trypsinized to single cells, and the above experimental procedure without nucleus staining was performed to analyze the quantification of proliferating cells by flow cytometry.

Cellular Uptake by NPCs in vitro

Confocal microscopy and TEM were used to observe the distribution of LDH in NPCs. 1 mg mL^{-1} FITC was incubated with 2 mg mL^{-1} MgAl-LDH overnight at 4°C in dark to label nanoparticles. NPCs treated with nanoparticles-FITC for 24 h were seeded on 24-well plate slides, fixed with 200 μL 4% PFA for 15 min, permeabilized with 200 μL 0.5% Triton X-100 for 20 min, incubated with Lyso red or Mito red (KeyGEN BioTECH, Nanjing) for 30 min, stained by 200 μL DAPI at 37°C for 15 min in dark, washed thrice with PBS, and finally the fluorescence of NPCs were photographed via confocal microscopy.

To analyze the cell sections by TEM, 40 μg mL^{-1} MgAl-LDH of all sizes were applied to incubate with cells for 24 h. The cells were then harvested and fixed overnight at 4°C with 2.5% glutaraldehyde, followed by 1% osmic acid for 1 h. After dehydration, the samples were embedded and sliced in an ultrathin microtome. The sections were then placed on copper grids and observed by TEM.

qRT-PCR Analysis

Cells were lysed by RNAiso Reagent (Takara) on the seventh day of differentiation to extract total RNA. Its concentration was quantified using Nanodrop. RNA processed by SPARKscript II RT Plus kit (with gDNA Eraser) (Sparkjade Biotechnology, Shandong) was reversed to cDNA. TB Green Premix Ex Taq (Takara) was applied to perform qRT-PCR analyses. The qPCR primers used in the experiments were listed in Table S1, Supporting information.

Western Blotting

Protein extraction kit (KeyGEN BioTECH, Nanjing) was used to extract proteins from cells, and extracted proteins were quantified using BCA protein assay kit (KeyGEN BioTECH, Nanjing) according to the kits' instructions. Quantitative protein samples supplemented with equal 2× loading buffer were boiled at 100°C for 10 min, and 20 μg protein samples were loaded and separated by SDS-PAGE gels, transferred to a PVDF membrane (Millipore, USA) that had been soaked in methanol for 1 min, blocked in 7.5% nonfat milk at room temperature for 1 h and soaked in specific primary antibody solution diluted with 5% BSA overnight at 4°C. The primary antibodies used in Western blot were listed as follows: SOX1, PAX6, N-CADHERIN were purchased from Abcam (CA, USA). The membranes were washed three times with TBST for 15 min, incubated with second antibody diluted with 7.5% nonfat milk at room temperature for 1 h, and washed three times with TBST for 15 min. Prepared ECL solution (Millipore, USA) was evenly dropped on the membranes, and then target bands were observed by chemiluminescence detection system (Tanon, Shanghai).

Immunofluorescent Staining

Spheres attached on 24-well plate slides were fixed in 200 μL 4% PFA for 20 min, permeabilized and blocked in 200 μL 10% normal donkey serum diluted with 0.5% Triton X-100 for 1 h, and incubated with 200 μL specific primary antibodies diluted with normal donkey serum and 0.1% Triton X-100 overnight at 4°C. Subsequently, cells were washed three times by PBS for 5 min and incubated with 200 μL fluorescent secondary antibodies diluted with normal donkey serum and 0.1% Triton X-100 at room temperature for 1 h in the dark. Then, the samples were stained by 200 μL DAPI at 37°C for 15 min without light and washed thrice by PBS for 5 min before the fluorescence of NPCs were observed and photographed via confocal microscopy (Zeiss, Germany).

Genes Knock-Down in mESCs

The generation of shMettl3-1 and shMettl3-2 was designed by Ribobio. shMettl3-1 and shMettl3-2 was transfected into mESCs using the typical lentiviral infection protocol. The cells were seeded at low density and treated with puromycin for 48 h after transfection.

Alkaline Phosphatase (ALP) Staining

ALP staining was used to observe the effect of *Mettl3* knockdown on the stemness of mESCs. mESCs were fixed in 4% PFA for 10 min, incubated with ALP working buffer for 20 min and observed by bright-field microscopy.

Embryoid Bodies (EBs) Formation

mESCs were dissociated by trypsin and cultured without LIF at a density of 5×10^4 cells mL^{-1} in ultra low attachment dishs for 5 d. As the EBs-like spheres formed, total RNA of shMettl3-1 and shMettl3-2 groups was extracted to detect markers expression of three germ layers.

Dot Blot

RNA samples at a concentration of approximately 500 ng μL^{-1} were incubated in a water bath at 65°C for 10 min and then placed on ice immediately after denaturation. Subsequently, 1 μL samples were dropped on a dried nylon membrane presoaked with TBST. The membrane spotted by denatured RNA samples was irradiated with ultraviolet for 30 min. The membrane was stained by methylene blue, washed by TBST for 10 min, blocked in 7.5% nonfat milk at room temperature for 1 h, and immersed with m^6A antibody solution diluted in 5% BSA overnight at 4°C. Subsequently, the membrane was washed thrice in TBST, then incubated with secondary antibody diluted in 7.5% nonfat milk at room temperature for 1 h. The membrane was then washed thrice in TBST and visualized by ECL solution (Sparkjade Biotechnology, Shandong) with a Tanon detection system.

Prediction of Sox1 and Pax6 M^6A Methylation Sites

The SRAMP tool, a m^6A modification site predictor, was used to predict the possible sites modified by m^6A. The entire sequence of Sox1 and Pax6 mRNA was uploaded to the server, and this tool automatically exported the possible m^6A methylation sites.

M^6A-RT-PCR (MeRIP-qPCR)

The total RNA extracted with RNAiso Reagent was used for MeRIP-qPCR. After fragmenting RNA, 1 μg of RNA was regarded as input group to immediately reverse to cDNA. The remaining 20 μg of RNA was used for subsequent immunoprecipitation experiments according to the instruction of GenSeq® m^6A MeRIP kit (Cloudseq, Shanghai). The primers used in MeRIP-qPCR were exhibited as follows: PF: TTTTCTCGGCTTCGGAGGAC; PR: AGAGCTGGCGGGAAGTAAAC.

RNA Stability Assays

To assess RNA stability, NPCs were treated with actinomycin D (Act-D) at a concentration of 5 μg mL^{-1}. The cells were incubated with Act-D at 37°C for 4 h. Subsequently, RNA was extracted from the samples using RNAiso Reagent for qPCR.

Statistical Analysis

The data presented in this study were the mean ± standard deviation of more than three independent replicates. Statistical significance was determined using one-way analysis of variance (ANOVA) with GraphPad Prism 6.

Results

Characterization of MgAl-LDH Nanoparticles

MgAl-LDH nanoparticles of three different sizes all exhibited regular layered hexagonal as shown in TEM images (Figure 1A), and high-resolution TEM images presented that the lattice fringes of MgAl-LDH with different diameters were 0.15 nm, 0.16 nm, and 0.22 nm in size, respectively (Figure 1B). Zetasizer was performed to detect surface charges of MgAl-LDH, and the mean Zeta potential of MgAl-LDH with different sizes was detected as 9.21 mV, 11.46 mV, and 20.9 mV, respectively (Figure 1C). The positive charge of nanoparticles promoted their adhesion to cell membranes that possessed negative charge. The peaks of elemental composition in LDH were detected using XPS. MgAl-LDH with three different sizes all possessed Mg 1s, Al 2p, N 1s, and O 1s peaks (Figures 1D and S1). MgAl-LDH of three different sizes presented characteristic (003) and (006) peaks as shown in XRD spectrum, demonstrating the layered structure of each type of MgAl-LDH was successfully constructed (Figure 1E).

Biocompatibility of MgAl-LDH Nanoparticles in NPCs

As shown in Figure 2A, the cell counting kit-8 was applied to evaluate the effects of MgAl-LDH of different sizes on NPCs. The result showed that 10~40 μg mL^{-1} MgAl-LDH of different sizes barely affects cell viability and there were no obvious differences in cell viability among all samples. The reports suggested that this concentration range was commonly used for LDH treatment of stem cells.[23,34] Hence, 40 μg mL^{-1} MgAl-LDH of different sizes were selected for the following research. The proliferation of NPCs treated with MgAl-LDH of different sizes was analyzed by EdU proliferation assay (Figure 2B). The fluorescence intensities of EdU were similar among all groups, indicating the proliferation of NPCs was not affected by LDH of different sizes. Furthermore, NPCs could maintain the typical sphere morphology after nanoparticles of different sizes treatment, and the size and amount of spheres barely decreased (Figure 2C).

The amounts of proliferating NPCs were evaluated by flow cytometry using the EdU proliferation kit. As shown (Figure 3A), bare of differences in the percentage of proliferating cells were detected among all samples. The Annexin V-APC/7-AAD apoptosis detection kit was used to detect whether MgAl-LDH of different sizes would induce the apoptosis of NPCs, and the result showed that the apoptosis rate of all groups was lower than 5%, and little differences in the ratio of apoptosis were detected between MgAl-LDH of different sizes treated samples and untreated samples (Figure 3B). Flow cytometer was also performed to analyze cell cycle in LDH treated NPCs, and the result indicated that MgAl-LDH of different sizes barely affected the distribution of cell cycle (Figure 3C). Furthermore, cellular uptake results showed that the majority of LDH signal spots overlapped with mitochondrial and lysosomal organelles, and the distribution of LDH in NPCs was clearly observable via TEM (Figure 4A and B).

Regulation of NPCs Differentiation by MgAl-LDH Nanoparticles

The expression of NPCs markers in cells treated with nanoparticles of different sizes was detected by qPCR. The expression level of differentiation markers (*Sox1, Pax6, N-cadherin* and *Map2*) of cells treated by LDH exhibited significant size-dependency, and the expression of NPCs markers in 100 nm MgAl-LDH group was significantly higher than other groups, demonstrating that 100 nm MgAl-LDH could effectively promote NPCs differentiation (Figure 5A). Western blot was used to analyze the changes in protein expression following LDH treatment, and SOX1, PAX6, and N-CADHERIN expression in LDH-treated groups also displayed significant size-dependency. Protein expression of NPCs markers in 100 nm MgAl-LDH group was significantly higher than other groups (Figures 5B and S2). These data indicated that 100 nm MgAl-LDH was superior to 30 nm and 50 nm MgAl-LDH in promoting the differentiation of mESCs into NPCs. Furthermore, we carried out immunofluorescence analysis to verify the promoted NPCs differentiation by MgAl-LDH with different size. It was noted that the fluorescence intensity of differentiation genes in 100 nm

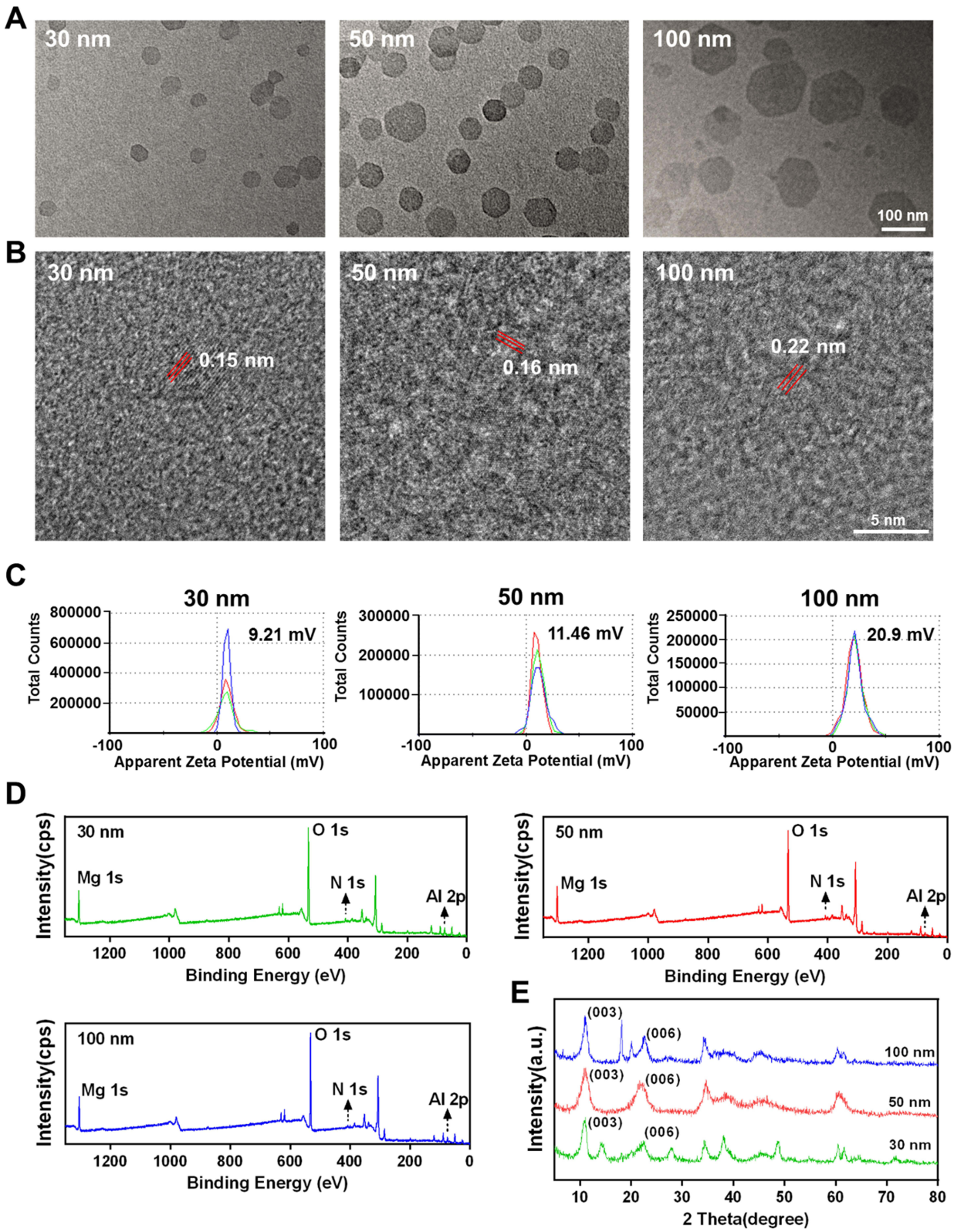

Figure 1 Characterization of LDH with different sizes. (**A**) TEM images of 30 nm, 50 nm and 100 nm LDH. (**B**) High-resolution TEM images of 30 nm, 50 nm, and 100 nm LDH. (**C**) Mean Zeta potential of 30 nm, 50 nm, and 100 nm LDH. (**D**) XPS spectrum of elemental composition in LDH with different sizes. (**E**) XRD spectrum of 30 nm, 50 nm, and 100 nm LDH.

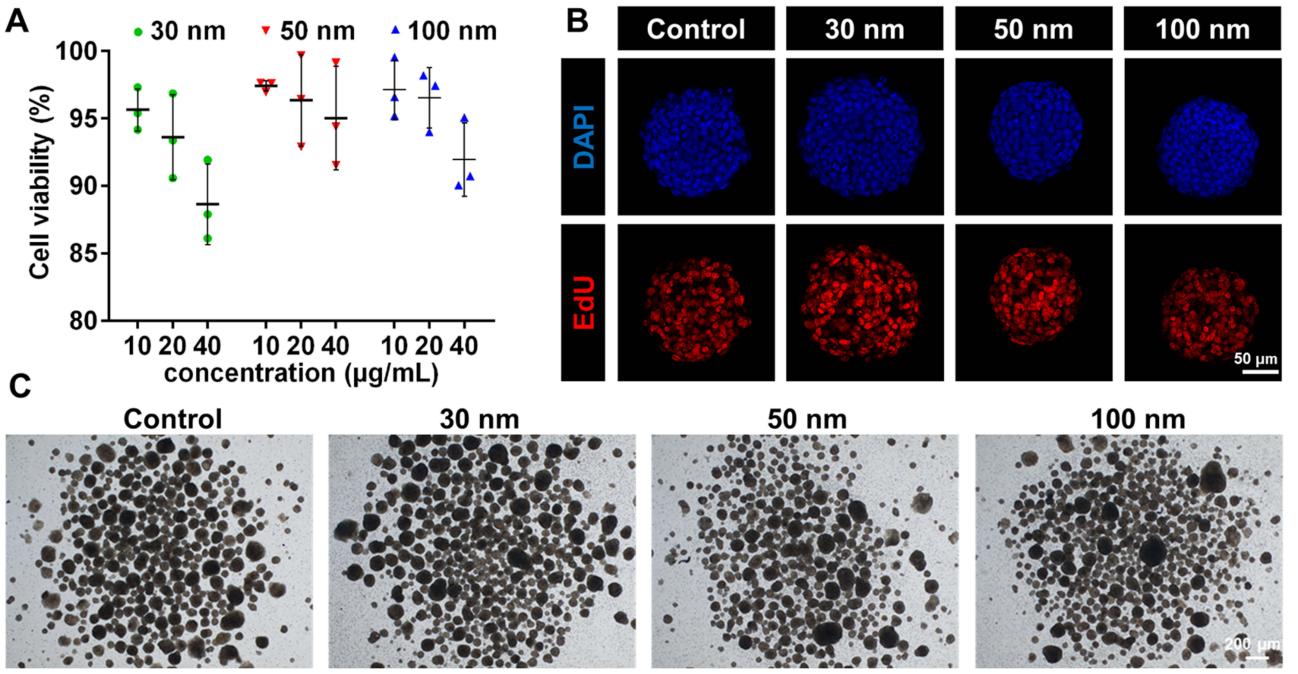

Figure 2 Influence of LDH with different sizes on cell viability, proliferation and morphology. (**A**) CCK8 detects the cell viability of NPCs treated with 30 nm, 50 nm and 100 nm LDH for 72 h. (**B**) EdU proliferation assay evaluates the proliferation of NPCs treated with 30 nm, 50 nm, and 100 nm LDH for 72 h. (**C**) Cell morphology of NPCs treated with 30 nm, 50 nm, and 100 nm LDH for 72 h.

MgAl-LDH group was stronger than that in the other groups (Figures 5C and S3). Hence, the 100 nm LDH was selected for the following research.

M^{6}A RNA Methylation is Required for Differentiation of mESCs into NPCs

It had been previously demonstrated that m^{6}A RNA modification could affect the fate of mESCs.[31,32] As depicted in Figure 5D and E, dot blot results displayed that the level of m^{6}A gradually increased with the progress of NPCs differentiation, and the level of m^{6}A in MgAL-LDH group on the seventh day of differentiation was significantly higher than that in the control group, demonstrating the enhanced NPCs differentiation by LDH may be closely related to m^{6}A methylation process. Furthermore, qPCR was used to analyze the level of RNA methylation-related enzymes (methyltransferases: METTL3, METTL14, WTAP, and demethylases: FTO, ALKBH5) in LDH-treated cells. The expression of *Mettl3* in MgAl-LDH group was significantly increased when compared with control group (Figure 5F), and there were bare differences in the expression levels of the other RNA methylation-related enzymes between control and LDH group, indicating the major modification enzyme in promoted NPCs differentiation by LDH may be the m^{6}A RNA methyltransferase METTL3.

M^{6}A methylation plays an important role in mouse embryonic stem cell differentiation. *Mettl3* knock down in cell lines will reduce the m^{6}A methylation level of most sites, leading to embryonic stem cell differentiation disorders.[35] shRNA-mediated downregulation of *Mettl3* in mESCs was performed to further characterize m^{6}A methylation of the process of mESCs differentiate to NPCs. The shMettl3 cell lines exhibited substantial knockdown of *Mettl3* RNA and protein (Figures 6A, B and S4). As depicted in Figure 6C, the expression of ESCs pluripotency markers (*Esrrb, Oct4, Rex1* and *Nanog*) was not suppressed by *Mettl3* deficiency. The pluripotency state of mESCs was commonly investigated by ALP staining. The clones of LIF-group displayed spontaneous differentiation and lower ALP activity compared with LIF+ group, whereas the clones of shMettl3-1 and shMettl3-2 group possessed similar ALP activity to LIF+ group (Figure 6D). The results indicated that downregulation of *Mettl3* had no substantial effect on the maintenance of mESCs pluripotency. Differentiation potential of mESCs was commonly detected by EBs in vitro. qPCR was performed to analyze marker genes expression of three germ layers formed in EBs. The gene levels of three germ layers in shMettl3-1 and shMettl3-2 group were substantially lower than those in shControl group, especially ectodermal genes associated with neurodevelopment (Figure 6E). Subsequently, the effect of *Mettl3* knockdown on LDH regulated NPCs differentiation was detected. As depicted (Figure 7A), the expression of NPCs markers in shMettl3-1 and shMettl3-2 group was

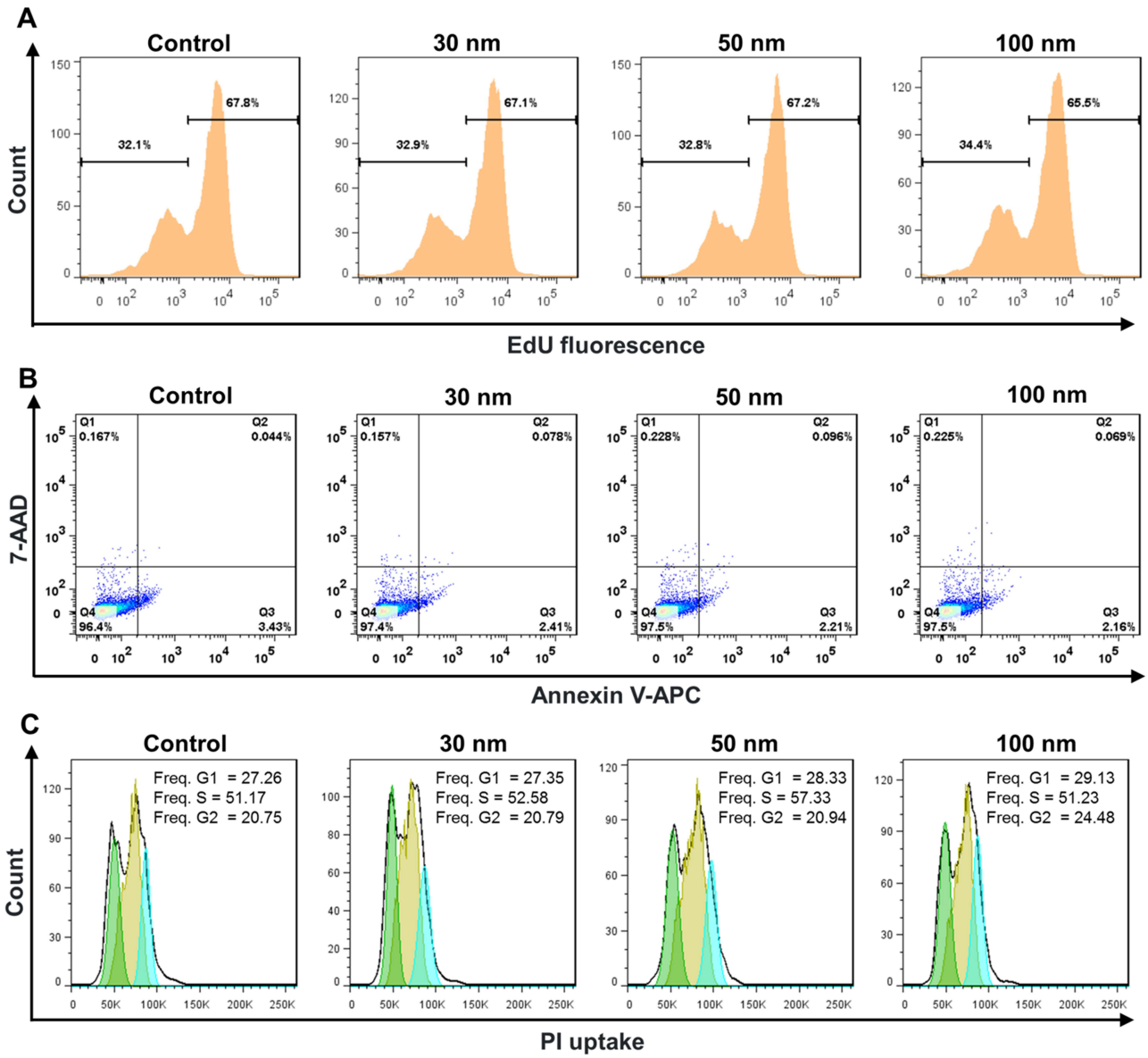

Figure 3 FACS detection of proliferation, apoptosis and cell cycle of NPCs treated by LDH with different sizes. (**A**) Quantification of proliferating NPCs treated with 30 nm, 50 nm, and 100 nm LDH for 72 h by FACS analysis. (**B**) FACS detection of apoptosis of NPCs treated with 30 nm, 50 nm, and 100 nm LDH for 72 h. (**C**) FACS detection of cell cycle variation in NPCs treated with 30 nm, 50 nm, and 100 nm LDH for 72 h.

significantly lower than the shControl group. *Mettl3* deficiency substantially reduced the fluorescence intensity of differentiation genes compared with the shControl group (Figures 7B and S5). These results demonstrated that downregulation of *Mettl3* significantly inhibited the differentiation of mESCs into NPCs. The shMettl3+LDH group exhibited similar mRNA expression and fluorescence intensity of differentiation markers to the shMettl3 group, indicating *Mettl3* deficiency affected the regulation of NPCs differentiation by LDH (Figure 7A and B).

LDH Upregulates the M^{6}A Level of Sox1 mRNA and Slows Down the Degradation of Sox1 mRNA

The effect of *Mettl3* knockdown on m^{6}A level regulated by LDH was also detected. Dot blot results showed that the m^{6}A level of shMettl3+LDH group similar to shMettl3 group was lower than shControl group, indicating *Mettl3* deficiency inhibited the upregulation of m^{6}A level by MgAL-LDH (Figure 8A). During the early stages of mouse embryonic neurogenesis, the transcription factors *Sox1* and *Pax6* are expressed in a sequential manner. The expression of *Sox1* appears first in the neural

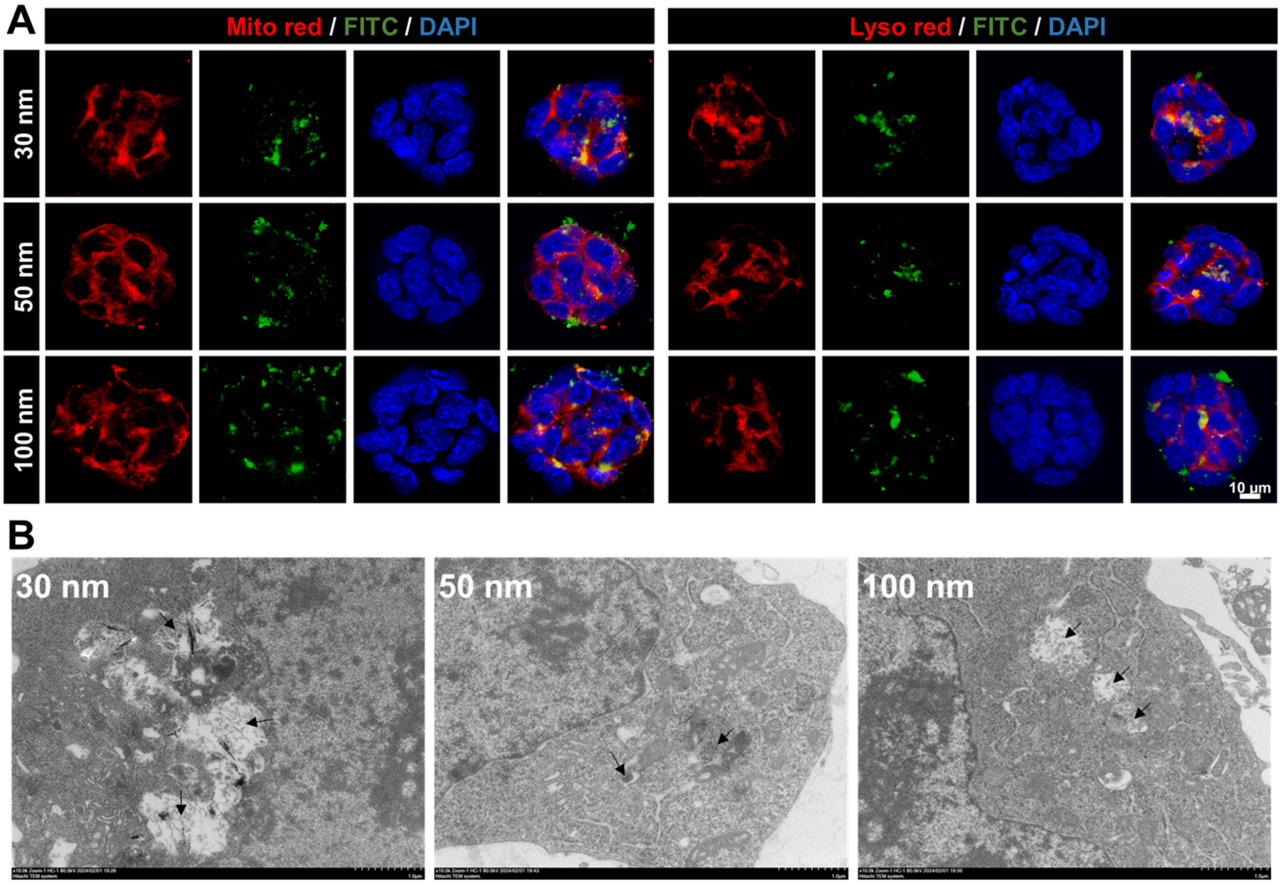

Figure 4 Internalization of LDH of all sizes in NPCs. (**A**) Cellular uptake of 30 nm, 50 nm, and 100 nm LDH in organelles of mitochondria and lysosomes. (**B**) TEM images of intracellular LDH of all sizes (black arrows) in NPCs.

ectoderm of mice, while *Pax6* expression responsible for the majority of neurons in the cerebral cortex commences in radial glial cells.[36] The possible sites of *Sox1* and *Pax6* mRNA modified by m^6A were predicted by SRAMP tool. As depicted in Figure 8B, there were 7 and 5 sites modified by m^6A with very high possibility in *Sox1* and *Pax6* mRNA, respectively. Sites modified by m^6A with very high possibility in *Sox1* mRNA possessed much higher combined score than that in *Pax6* mRNA (Tables S2 and S3). Hence, *Sox1* was selected for following MeRIP-qPCR. We selected the 2217th site of *Sox1* mRNA as target site for designing specific primers. Our findings suggested that LDH significantly upregulated the m^6A level of *Sox1*, which may result in increased expression level of *Sox1* (Figure 8C). *Mettl3* deficiency suppressed the upregulation of m^6A level of *Sox1* by LDH (Figure 8D). Researches have shown that m^6A methylation modification can affect the stability of RNA, thus affecting RNA function.[29] Subsequently, Act-D, an RNA polymerase II inhibitor, was used to investigate the impact of increased m^6A level on the stability of *Sox1* mRNA. The results demonstrated that the degradation of *Sox1* mRNA in LDH-treated cells significantly attenuated compared to control group, indicating a prolonged half-life (Figure 8E and F). The above data revealed that the increased m^6A level of *Sox1* mRNA by LDH may slow down the degradation of *Sox1* mRNA.

Discussion

In this work, we investigated the regulation of MgAl-LDH nanoparticles in the process of mESCs differentiate to NPCs. We conclusively proved that MgAl-LDH was capable of promoting the differentiation of mESCs into NPCs, closely related to m^6A methylation modification. Compared with other inorganic nanoparticles, LDH with controllable physicochemical properties and extremely low toxicity is easily synthesized and chemically well-defined.[37] LDH is commonly defined as $[M_{1-x}^{2+}M_x^{3+}(OH)_2][A_{x/n}]mH_2O$, and the common M^{2+} (divalent metal ions) and M^{3+} (trivalent metal ions) in LDH can be chosen from Mg^{2+}, Ni^{2+}, Zn^{2+}, Co^{2+} and Fe^{3+}, Al^{3+}, Ga^{3+}, Mn^{3+}, respectively, which enables researchers to optimize LDH according to

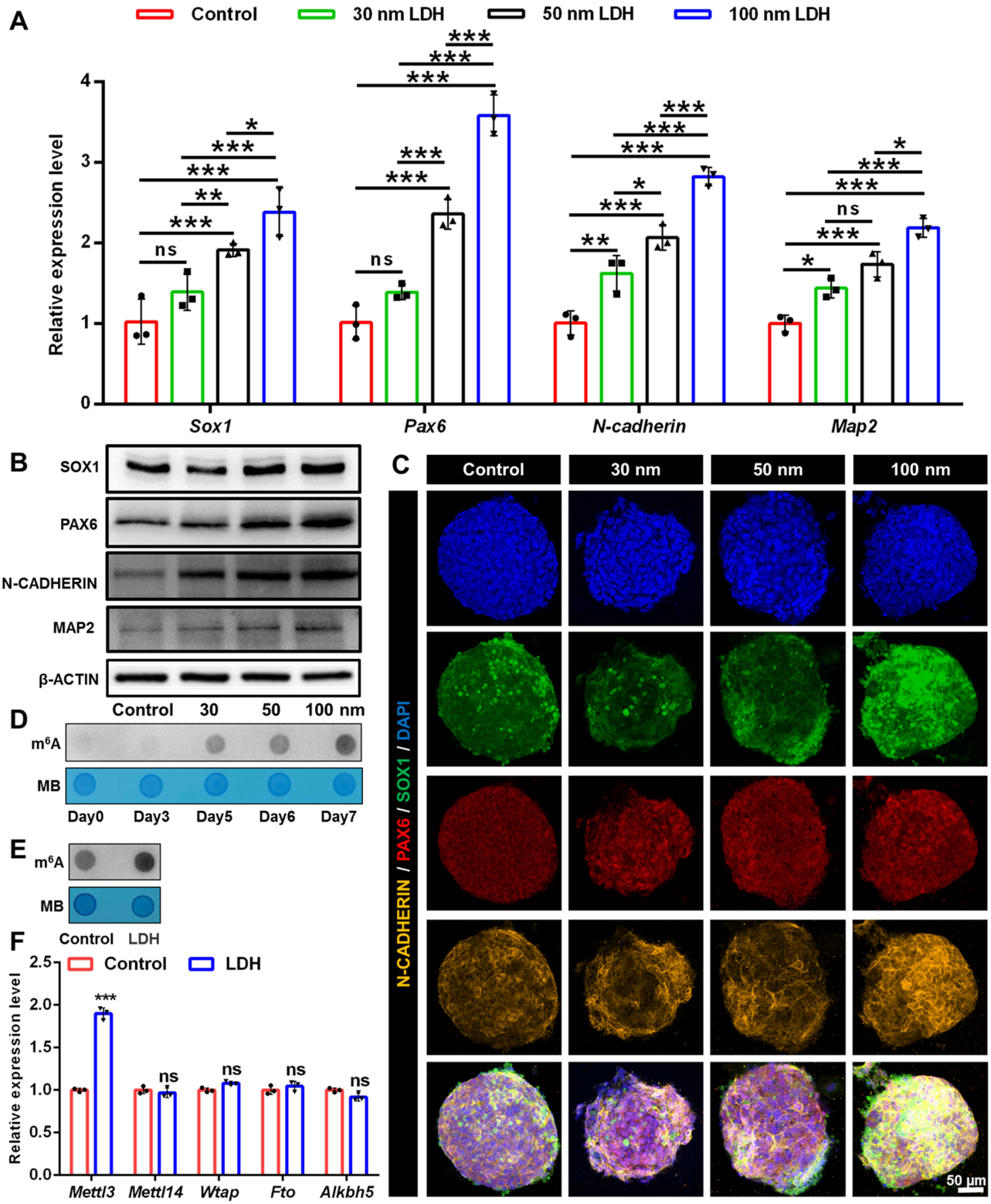

Figure 5 The effect of LDH with different sizes on NPCs differentiation and its relationship with m^{6}A RNA methylation. (**A**) qPCR analysis of the mRNA expression level of *Sox1*, *Pax6*, *N-cadherin* and *Map2* in NPCs treated by LDH with different sizes. (**B**) Western blot detects the protein expression of SOX1, PAX6, N-CADHERIN and MAP2 in NPCs treated by LDH with different sizes. (**C**) Immunofluorescence analysis of the expression level of SOX1, PAX6 and N-CADHERIN in NPCs treated by LDH with different sizes. (**D**) Dot blot analysis of the m^{6}A level in the progress of NPCs differentiation. (**E**) Dot blot analysis of the m^{6}A level in 100 nm LDH-treated NPCs on the 7th day of differentiation. (**F**) qPCR analysis of the mRNA expression level of *Mettl3, Mettl14, Wtap, Fto* and *Alkbh5* in 100 nm LDH-treated NPCs. The data are presented as the mean ± SD (n=3, ***p < 0.001, **p < 0.01, *p < 0.05, ns means there was no significant difference between the two groups).

https://doi.org/10.2147/IJN.S463141 DovePress

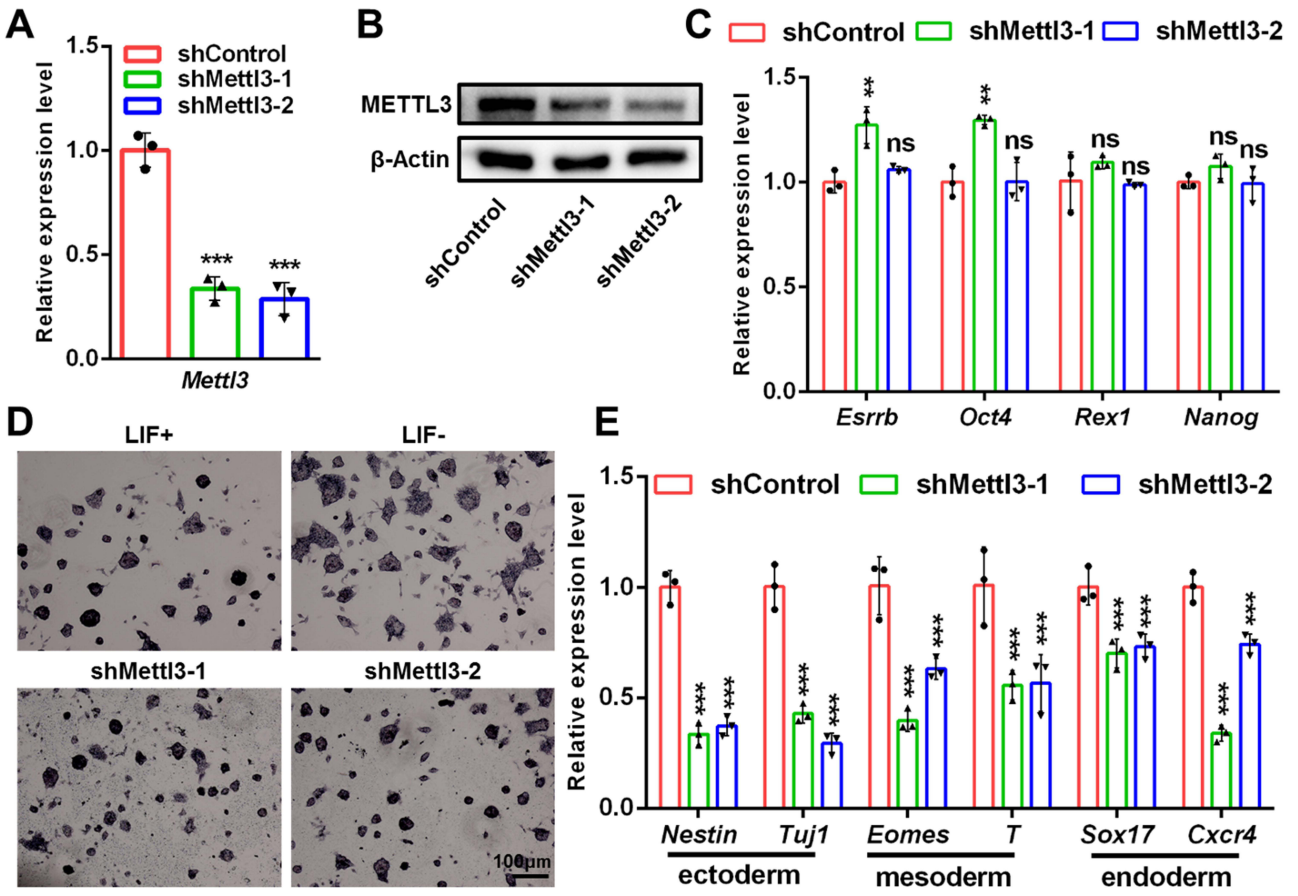

Figure 6 The effect of Mettl3 deficiency on stemness and pluripotency of mESCs. (**A**) qPCR analysis of the mRNA expression level of *Mettl3* in shMettl3 cell lines. (**B**) Western blot detects the protein expression of METTL3 in shMettl3 cell lines. (**C**) qPCR detects the effect of *Mettl3* deficiency on the mRNA expression level of *Esrrb, Oct4, Rex1* and *Nanog* in mESCs. (**D**) ALP staining detects the effect of *Mettl3* deficiency on the pluripotency of mESCs. (**E**) qPCR detects the effect of *Mettl3* deficiency on the mRNA expression level of three germ layers markers in EBs. The data are presented as the mean ± SD (n=3, ***p < 0.001, **p < 0.01, *p < 0.05, ns means there was no significant difference between the two groups).

specific experimental requirements.[38] Diverse permutations and combinations of M^{2+} and M^{3+} in LDH endow it with unlimited application potential. In this study, we selected Al^{3+} and synthesized MgAl-LDH nanoparticles.

Increasing researches indicated that LDH could be used to regulate the fate of stem cell differentiation. Cheng et al revealed that LDH could promote neural stem cells migration and neural differentiation by targeting transforming growth factor-β receptor 2, and the nanocomposite system formed by loading neurotrophic factor NT3 onto LDH could effectively restore the motor function of spinal cord injury mice.[24] Zhang et al designed a LDH-doped gelatin-chitosan scaffold with aligned microchannels (GC-LDH/A), and found that the GC-LDH/A scaffold facilitated the neural differentiation of neural stem cells, axonal growth, and recovered motor function of spinal cord injury mice by suppressing the activity of myosin II.[39] The physical properties of nanomaterials are determined by their microscopic structure and size. In recent years, the regulation of stem cell fate using the physical properties of materials, such as shape and particle size, has become a key research direction in the fields of tissue engineering and regenerative medicine. Some studies suggested that the particle size of nanomaterials could affect the differentiation and proliferation of stem cells.[40–42] In this work, MgAl-LDH nanoparticles of different sizes with specific lamellar morphology were observed to be hexagonal, and biocompatible MgAl-LDH nanoparticles barely affect cell cycle, proliferation, apoptosis, and morphology of NPCs. The addition of LDH could significantly facilitated the differentiation of mESCs into NPCs, and the promoted NPCs differentiation showed significant size-dependency, demonstrated by increased expression levels of genes and proteins associated with NPCs differentiation.

Studies have shown that m^6A methylation modification plays an important role in the fate of mouse embryonic stem cells.[43] Although no reports had shown a direct correlation between the size of nanoparticles and m^6A RNA methylation. However, the size of the nanoparticles may affect their uptake and distribution within the cells, thus affecting the m^6A modification of RNA.

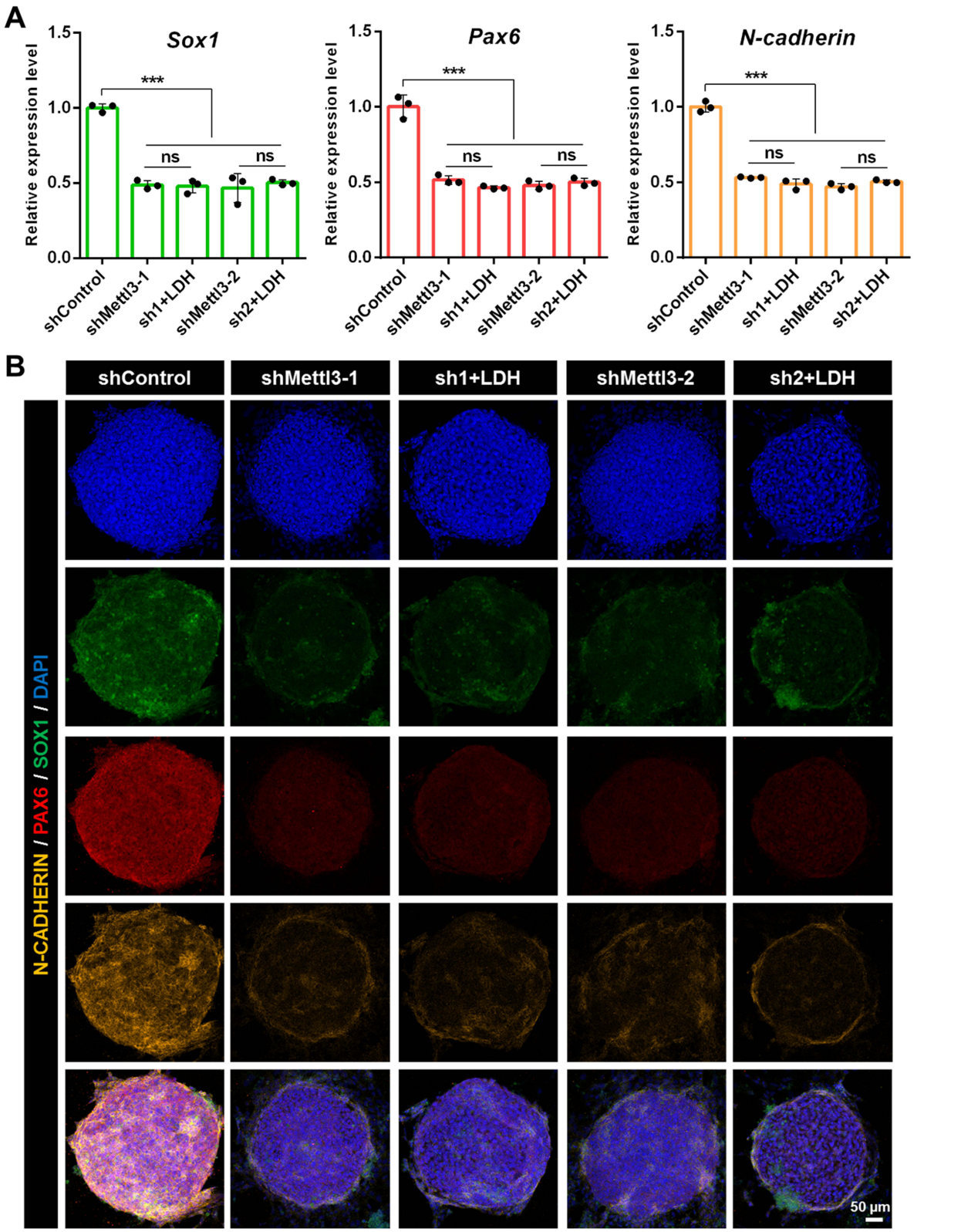

Figure 7 The effect of Mettl3 deficiency on NPCs differentiation of mESCs. (**A**) qPCR analysis of the effect of *Mettl3* deficiency on the mRNA expression level of *Sox1*, *Pax6* and *N-cadherin* in LDH-treated NPCs. (**B**) Immunofluorescence analysis of the effect of *Mettl3* deficiency on the expression level of SOX1, PAX6 and N-CADHERIN in LDH-treated NPCs. The data are presented as the mean ± SD (n=3, ***p < 0.001, ns means there was no significant difference between the two groups).

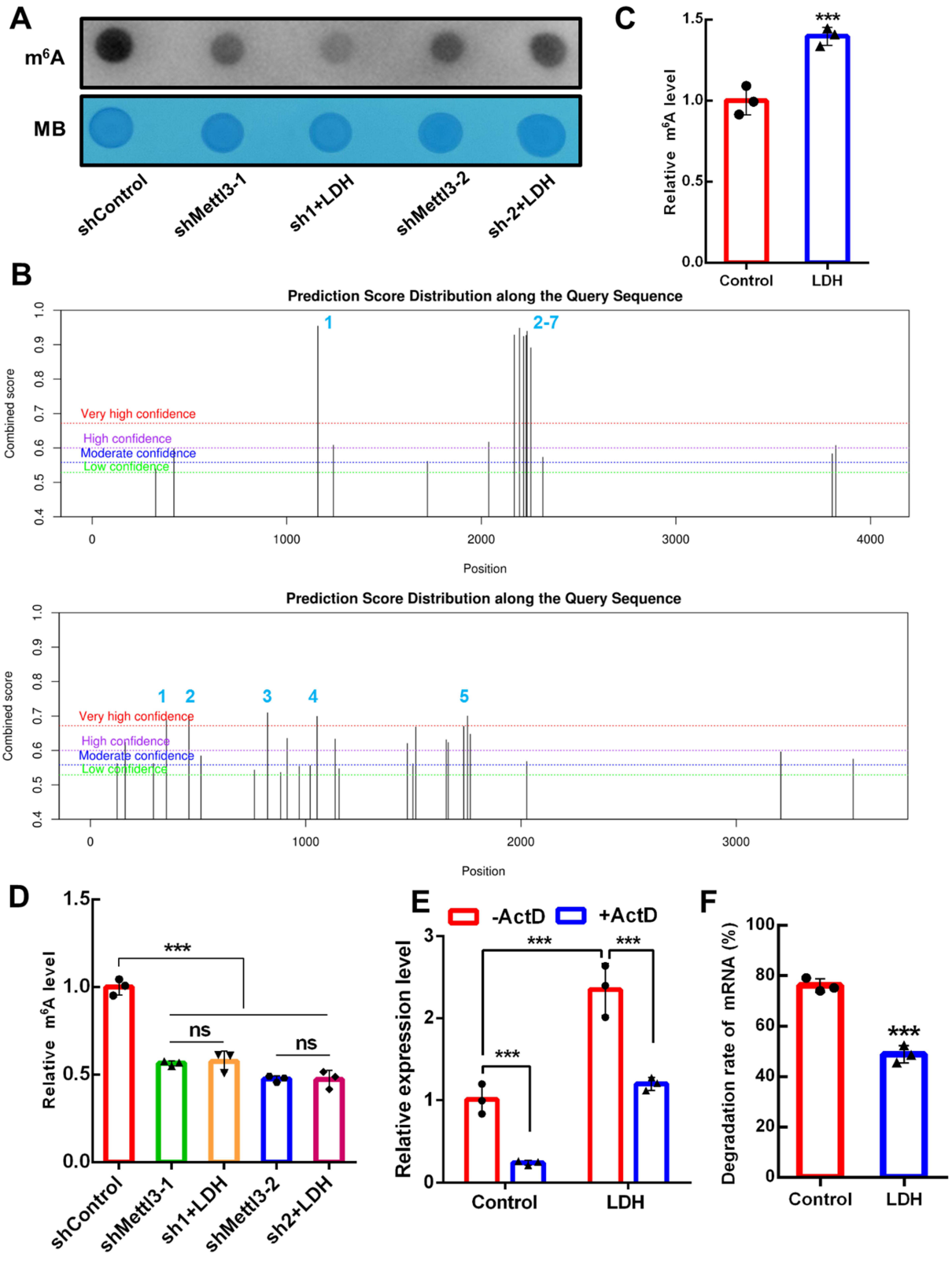

Figure 8 The m^{6}A level and stability of *Sox1* mRNA in LDH-treated NPCs. (**A**) Dot blot detects the effect of *Mettl3* deficiency on the m^{6}A level in LDH-treated NPCs. (**B**) Possible sites with m^{6}A modification of *Sox1* (up) and *Pax6* (down) mRNA. (**C**) M^{6}A level of *Sox1* mRNA in LDH-treated NPCs. (**D**) The effect of *Mettl3* deficiency on the m^{6}A level of *Sox1* mRNA in LDH-treated NPCs. (**E**) qPCR detects the mRNA expression level of *Sox1* after Act-D treatment. (**F**) The degradation rate of *Sox1* mRNA after Act-D treatment. The data are presented as the mean ± SD (n=3, ***p < 0.001, ns means there was no significant difference between the two groups).

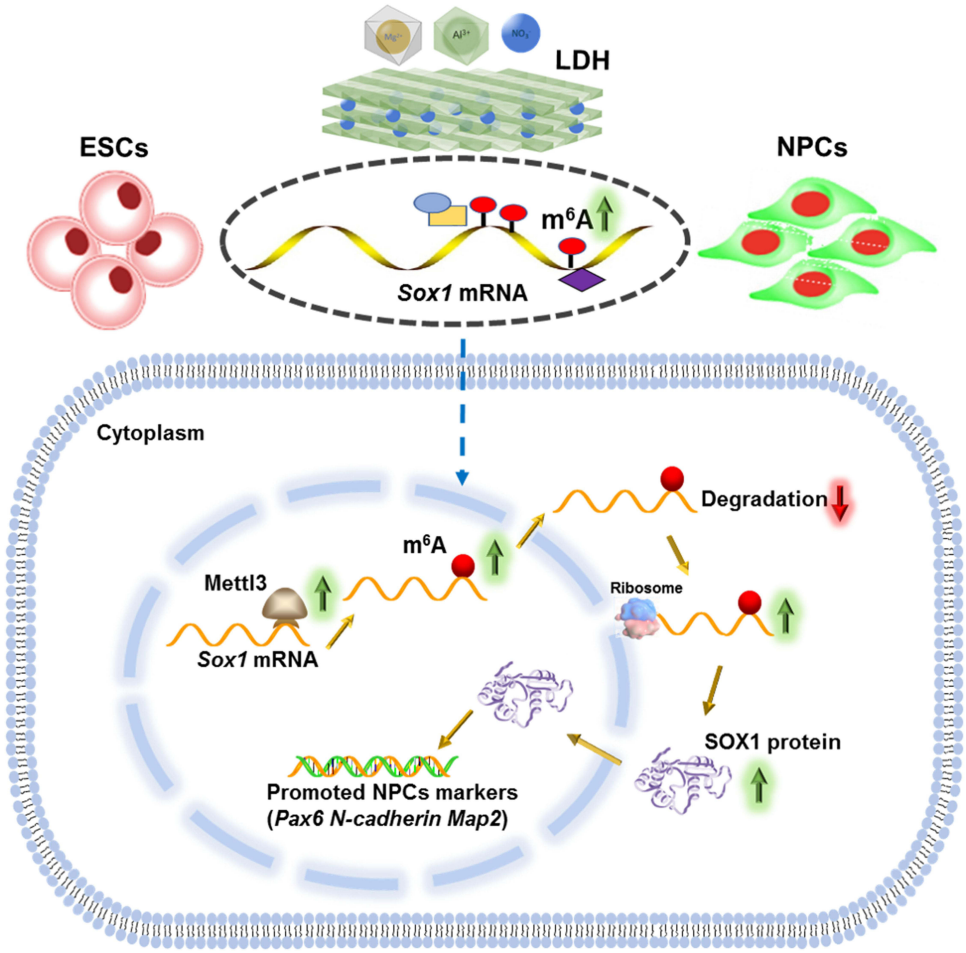

Figure 9 Schematic diagram of LDH regulating NPCs differentiation of mouse embryonic stem cells.

Furthermore, nanoparticles may indirectly influence m^6A modification by affecting intracellular metabolic pathways, signaling pathways, or RNA modification enzyme activity. The gradual increased m^6A level during the process of ESC differentiation into NPCs and the enhanced level of m^6A RNA methylation in LDH-treated NPCs indicated that MgAl-LDH could promote NPCs differentiation via regulating m^6A modification. Furthermore, we found that the expression level of *Mettl3* in MgAl-LDH group was significantly higher than that of control group, and the expression levels of the other m^6A methylation-related enzymes were not significantly affected after LDH treatment, indicating the m^6A methyltransferase METTL3 may be the specific modification enzyme in LDH regulated NPCs differentiation. METTL3 is an m^6A methyltransferase on mRNA that mainly participates in the fate regulation of mRNA.[44] Few researches had been reported about the mechanism of METTL3 in neural precursor cell differentiation of mESCs. Our results showed that downregulation of *Mettl3* barely affected mESCs pluripotency, whereas significantly depressed EBs differentiation of mESCs, especially ectoderm associated with neurodevelopment (Figure 6). In addition, *Mettl3* deficiency also significantly suppressed the differentiation of mESCs into NPCs and the promotion effect of LDH on NPCs (Figure 7).

Taken together, the MgAl-LDH nanoparticles in this paper possessed excellent support for the differentiation of mESCs into NPCs by the elevation of m^6A level of *Sox1*. This study exhibits notable insights into the significance of the promotion of MgAl-LDH nanoparticles on NPCs differentiation, offering theoretical basis for the cell fate regulation of biomaterials in ESCs at the epigenetic level.

Conclusion

In this work, the effect of LDH on the NPCs differentiation of ESCs, and the association between promoted differentiation by LDH and m^6A methylation modification were investigated. Our findings suggested that the promoted NPCs

differentiation by LDH with different sizes showed significant size-dependency, and 100 nm LDH upregulated the expression level of METTL3, which led to increased m^6A level of *Sox1* mRNA. The enhanced m^6A level was conductive to the stability of *Sox1* mRNA, resulting in upregulated *Sox1* mRNA and protein levels. As a result, SOX1 promoted the transcription of other NPCs markers, and then enhanced NPCs differentiation of ESCs (Figure 9).

Acknowledgments

This work was financially supported by the National Natural Science Foundation of China (Grant No. 82225027, 82202702, 82202351, 82301550, 82271418, 82001308, 82202803, and 82271419), the National Key Research and Development Program (Grant No. 2021YFA1101301), the Fundamental Research Funds for the Central Universities (Grant No. 22120230292, 22120220555, and 22120240163), the China Postdoctoral Science Foudation (2023M742647), and Shanghai Rising-Star Program (Grant No. 22QA1408200).

Disclosure

The authors report no conflicts of interest in this work.

References

1. Li Y, Mao X, Zhou X, et al. An optimized method for neuronal differentiation of embryonic stem cells in vitro. *J Neurosci Methods*. 2020;330:108486. doi:10.1016/j.jneumeth.2019.108486
2. Wang Z, Yang H, Bai Y, et al. rBMSC osteogenic differentiation enhanced by graphene quantum dots loaded with immunomodulatory layered double hydroxide nanoparticles. *Biomed Mater*. 2022;17(2):024101. doi:10.1088/1748-605X/ac4324
3. Ogawa Y, Sawamoto K, Miyata T, et al. Transplantation of in vitro-expanded fetal neural progenitor cells results in neurogenesis and functional recovery after spinal cord contusion injury in adult rats. *J Neurosci Res*. 2002;69(6):925–933. doi:10.1002/jnr.10341
4. Iwai H, Shimada H, Nishimura S, et al. Allogeneic neural stem/progenitor cells derived from embryonic stem cells promote functional recovery after transplantation into injured spinal cord of nonhuman primates. *Stem Cells Transl Medi*. 2015;4(7):708–719. doi:10.5966/sctm.2014-0215
5. Chang DJ, Oh SH, Lee N, et al. Contralaterally transplanted human embryonic stem cell-derived neural precursor cells (ENStem-A) migrate and improve brain functions in stroke-damaged rats. *Exp Mol Med*. 2013;45(11):e53. doi:10.1038/emm.2013.93
6. Zeevaert K, Elsafi Mabrouk MH, Wagner W, et al. Cell mechanics in embryoid bodies. *Cells*. 2020;9(10):2270. doi:10.3390/cells9102270
7. Shparberg RA, Glover HJ, Morris MB. Embryoid body differentiation of mouse embryonic stem cells into neurectoderm and neural progenitors. *Methods Mol Biol*. 2019;2019:273–285. doi:10.1007/978-1-4939-9631-5_21.
8. Joshi R, Buchanan JC, Tavana H. Self-regulatory factors of embryonic stem cells in co-culture with stromal cells enhance neural differentiation. *Integr Biol*. 2017;9(5):418–426. doi:10.1039/C7IB00038C
9. Rifes P, Isaksson M, Rathore GS, et al. Modeling neural tube development by differentiation of human embryonic stem cells in a microfluidic WNT gradient. *Nat Biotechnol*. 2020;38(11):1265–1273. doi:10.1038/s41587-020-0525-0
10. Zhang C, Du L, Pang K, et al. Differentiation of human embryonic stem cells into corneal epithelial progenitor cells under defined conditions. *PLoS One*. 2017;12(8):e0183303. doi:10.1371/journal.pone.0183303
11. Kang MK, Kim TJ, Kim YJ, et al. Targeted delivery of iron oxide nanoparticle-loaded human embryonic stem cell-derived spherical neural masses for treating intracerebral hemorrhage. *Int J Mol Sci*. 2020;21(10):3658. doi:10.3390/ijms21103658
12. Rahimi Darehbagh R, Mahmoodi M, Amini N, et al. The effect of nanomaterials on embryonic stem cell neural differentiation: a systematic review. *Eur J Med Res*. 2023;28(1):576. doi:10.1186/s40001-023-01546-0
13. Pinto MC, Tonelli FM, Vieira AL, et al. Studying complex system: calcium oscillations as attractor of cell differentiation. *Integr Biol*. 2016;8(2):130–148. doi:10.1039/c5ib00285k
14. Marques BL, Maciel GF, Brito MRJ, et al. Regulatory mechanisms of stem cell differentiation: biotechnological applications for neurogenesis. *Semin Cell Dev Biol*. 2023;144:11–19. doi:10.1016/j.semcdb.2022.09.014
15. Asgari V, Landarani-Isfahani A, Salehi H, et al. The Story of Nanoparticles in Differentiation of Stem Cells into Neural Cells. *Neurochem Res*. 2019;44(12):2695–2707. doi:10.1007/s11064-019-02900-7
16. Qiu J, Liu XJ, You BA, et al. Application of nanomaterials in stem cell-based therapeutics for cardiac repair and regeneration. *Small*. 2023;19(11):e2206487. doi:10.1002/smll.202206487
17. Gupta P, Rathi P, Gupta R, et al. Neuronal maturation-dependent nano–neuro interaction and modulation. *Nanoscale Horiz*. 2023;8(11):1537–1555. doi:10.1039/D3NH00258F
18. da Silva VA, Bobotis BC, Correia FF, et al. The impact of biomaterial surface properties on engineering neural tissue for spinal cord regeneration. *Int J Mol Sci*. 2023;24(17):13642. doi:10.3390/ijms241713642
19. Sperling LE, Reis KP, Pozzobon LG, et al. Influence of random and oriented electrospun fibrous poly(lactic-co-glycolic acid) scaffolds on neural differentiation of mouse embryonic stem cells. *J Biomed Mater Res A*. 2017;105(5):1333–1345. doi:10.1002/jbm.a.36012
20. Park SJ, Kim S, Kim SY, et al. Highly efficient and rapid neural differentiation of mouse embryonic stem cells based on retinoic acid encapsulated porous nanoparticle. *ACS Appl Mater Interfaces*. 2017;9(40):34634–34640. doi:10.1021/acsami.7b09760
21. Zhang S, Hang Y, Wu J, et al. Dual pathway for promotion of stem cell neural differentiation mediated by gold nanocomposites. *ACS Appl Mater Interfaces*. 2020;12(19):22066–22073. doi:10.1021/acsami.9b22258
22. Taviot-Gueho C, Prevot V, Forano C, et al. Tailoring hybrid layered double hydroxides for the development of innovative applications. *Adv Funct Mater*. 2018;28(27):1703868. doi:10.1002/adfm.201703868

23. He X, Zhu Y, Yang L, et al. MgFe-LDH nanoparticles: a promising leukemia inhibitory factor replacement for self-renewal and pluripotency maintenance in cultured mouse embryonic stem cells. *Adv Sci*. 2021;8(9):2003535. doi:10.1002/advs.202003535
24. Zhu R, Zhu X, Zhu Y, et al. Immunomodulatory layered double hydroxide nanoparticles enable neurogenesis by targeting transforming growth factor-β Receptor 2. *ACS nano*. 2021;15(2):2812–2830. doi:10.1021/acsnano.0c08727
25. Yang L, Sun J, Liu Q, et al. Synergetic functional nanocomposites enhance immunotherapy in solid tumors by remodeling the immunoenvironment. *Adv Sci*. 2019;6(8):1802012. doi:10.1002/advs.201802012
26. Zhao BS, Roundtree IA, He C. Post-transcriptional gene regulation by mRNA modifications. *Nat Rev Mol Cell Biol*. 2017;18(1):31–42. doi:10.1038/nrm.2016.132
27. Yang Y, Hsu PJ, Chen YS, et al. Dynamic transcriptomic m(6)A decoration: writers, erasers, readers and functions in RNA metabolism. *Cell Res*. 2018;28(6):616–624. doi:10.1038/s41422-018-0040-8
28. Lee M, Kim B, Kim VN. Emerging roles of RNA modification: m(6)A and U-tail. *Cell*. 2014;158(5):980–987. doi:10.1016/j.cell.2014.08.005
29. Han L, Dong L, Leung K, et al. METTL16 drives leukemogenesis and leukemia stem cell self-renewal by reprogramming BCAA metabolism. *Cell Stem Cell*. 2023;30(1):52–68.e13. doi:10.1016/j.stem.2022.12.006
30. Tooley JG, Catlin JP, Tooley CES. METTLing in stem cell and cancer biology. *Stem Cell Rev Rep*. 2023;19(1):76–91. doi:10.1007/s12015-022-10444-7
31. Batista PJ, Molinie B, Wang J, et al. m(6)A RNA modification controls cell fate transition in mammalian embryonic stem cells. *Cell Stem Cell*. 2014;15(6):707–719. doi:10.1016/j.stem.2014.09.019
32. Geula S, Moshitch-Moshkovitz S, Dominissini D, et al. m6A mRNA methylation facilitates resolution of naïve pluripotency toward differentiation. *Science*. 2015;347(6225):1002–1006. doi:10.1126/science.1261417
33. Xu W, Li J, He C, et al. METTL3 regulates heterochromatin in mouse embryonic stem cells. *Nature*. 2021;591(7849):317–321. doi:10.1038/s41586-021-03210-1
34. Wang Z, Xu Z, Jing G, et al. Layered double hydroxide eliminate embryotoxicity of chemotherapeutic drug through BMP-SMAD signaling pathway. *Biomaterials*. 2020;230:119602. doi:10.1016/j.biomaterials.2019.119602
35. Wu Y, Xu X, Qi M, et al. N(6)-methyladenosine regulates maternal RNA maintenance in oocytes and timely RNA decay during mouse maternal-to-zygotic transition. *Nat Cell Biol*. 2022;24(6):917–927. doi:10.1038/s41556-022-00915-x
36. Suter DM, Tirefort D, Julien S, et al. A Sox1 to Pax6 switch drives neuroectoderm to radial glia progression during differentiation of mouse embryonic stem cells. *Stem Cells*. 2009;27(1):49–58. doi:10.1634/stemcells.2008-0319
37. Wang Z, Yang H, Xu X, et al. Ion elemental-optimized layered double hydroxide nanoparticles promote chondrogenic differentiation and intervertebral disc regeneration of mesenchymal stem cells through focal adhesion signaling pathway. *Bioact Mater*. 2023;22:75–90. doi:10.1016/j.bioactmat.2022.08.023
38. Mao N, Zhou CH, Tong DS, et al. Exfoliation of layered double hydroxide solids into functional nanosheets. *Appl Clay Sci*. 2017;144(4):60–78. doi:10.1016/j.clay.2017.04.021
39. Zhang T, Wang Z, Wang Z, et al. LDH-doped gelatin-chitosan scaffold with aligned microchannels improves anti-inflammation and neuronal regeneration with guided axonal growth for effectively recovering spinal cord injury. *Appl Mater Today*. 2023;34:101884. doi:10.1016/j.apmt.2023.101884
40. Qiu J, Li J, Wang S, et al. TiO2 nanorod array constructed nanotopography for regulation of mesenchymal stem cells fate and the realization of location-committed stem cell differentiation. *Small*. 2016;12(13):1770–1778. doi:10.1002/smll.201503946
41. Qiu J, Li D, Mou X, et al. Effects of graphene quantum dots on the self-renewal and differentiation of mesenchymal stem cells. *Adv Healthcare Mater*. 2016;5(6):702–710. doi:10.1002/adhm.201500770
42. Li J, Qiu J, Guo W, et al. Cellular internalization of LiNbO3 nanocrystals for second harmonic imaging and the effects on stem cell differentiation. *Nanoscale*. 2016;8(14):7416–7422. doi:10.1039/C6NR00785F
43. Zhang C, Chen Y, Sun B, et al. m(6)A modulates haematopoietic stem and progenitor cell specification. *Nature*. 2017;549(7671):273–276. doi:10.1038/nature23883
44. Zhang ZW, Teng X, Zhao F, et al. METTL3 regulates m(6)A methylation of PTCH1 and GLI2 in Sonic hedgehog signaling to promote tumor progression in SHH-medulloblastoma. *Cell Rep*. 2022;41(4):111530. doi:10.1016/j.celrep.2022.111530